Effect of plasma treatment on LMPAEK/CF tape and composites manufactured by automated tape placement (ATP)

Georges Chahine[1*], Umesh Marathe[2*]‡, Liam Collins[3], Vinoy Thomas[4], Vipin Kumar[2], Ahmed Arabi Hassen[2], Halil Tekinalp[2], Soydan Ozcan[2] and Uday Vaidya [1,2,5]

1. Tickle college of Engineering, University of Tennessee, Knoxville, TN, 37996 USA
2. Manufacturing Sciences Division (MSD), Oak Ridge National Laboratory (ORNL), 2350 Cherahala Blvd, Knoxville, TN 37832, USA
3. Center for Nanophase Materials Sciences, Oak Ridge National Laboratory (ORNL), Oak Ridge, TN 37830, USA
4. Department of Mechanical and Materials Engineering, University of Alabama at Birmingham, (UAB), Birmingham, AL 35294
5. Institute for Advanced Composites Manufacturing Innovation, 10658 Checkerboard Lane, Knoxville, TN 37932, USA.

*Authors contributed equally

‡ Corresponding author, Email: maratheun@ornl.gov

Phone: +1 865 321 0838

ABSTRACT

Automated tape placement (ATP) process is widely used in aerospace for its advanced process control and multi-axis capabilities but faces issues like limited choice of materials and suboptimal tape consolidation. This study investigates air plasma treatment on ATP carbon fiber thermoplastic feedstock tape to address these challenges. The effects on low melt Polyaryletherketone/carbon fiber unidirectional tape (LMPAEK/CF UD tape) were analyzed. Treated and untreated tapes were used to fabricate composites and evaluated for physical, thermal, mechanical, and interfacial properties. Atomic force microscopy (AFM), X-ray photoelectron spectroscopy (XPS) and Fourier transform infrared (FTIR) analyses revealed surface roughness changes (on LMPAEK), extent of oxidation, and the presence of hydroxyl/carboxyl groups. Composites from plasma-treated tapes showed a 7.6% increase in tensile strength, 8% in tensile modulus, 18% in flexural strength, and 8.3% in flexural modulus. The interlaminar shear strength improved by 18.7%. Failure analysis showed untreated composites failed via inter-ply and fiber-matrix delamination, while treated composites

experienced matrix cracking and fiber breakage. This study highlights atmospheric plasma treatment as a solution to ATP's limitations, significantly enhancing LMPAEK/CF UD tape composites' properties.

1. INTRODUCTION

Composite materials are essential in engineering applications across industries such as aerospace, automotive, wind energy, and sports. The performance of composites relies on the interaction between three critical components: the matrix, reinforcement, and the interface. The matrix, which can be either metal or polymer (thermoset or thermoplastic), binds the reinforcement (particulate or fiber) and enhances the resulting mechanical properties like strength and stiffness. The interface between matrix and reinforcement is crucial for stress transfer and influences durability and mechanical performance [1-7]. Prior research emphasizes that the interfacial quality is affected by factors such as the reinforcement's size, surface chemistry, and physical features, including surface roughness. The performance properties of composite can be tailored for typical applications by leveraging surface modification treatments [8-14].

Surface modifications, particularly plasma treatments, have demonstrated the potential to improve interfacial bonding. For instance, Sharma et al. [15] showed that plasma treatments introducing hydroxyl groups on carbon fibers (CF) can enhance interfacial shear strength by 90%, significantly improving the stress transfer between fibers and the matrix. Further studies on surface treatments, including oxidation, nanoparticle deposition, and irradiation, corroborate the benefits of modifying carbon fiber surfaces to improve composite performance [16-18].

Automated Tape Placement (ATP) is a cutting-edge composite manufacturing technique employed to fabricate advanced aerospace components. ATP uses heat and pressure to lay pre-impregnated unidirectional (UD) tapes onto a mandrel, consolidating them in-situ. However, challenges remain in mitigating porosity and enhancing interfacial bonding, often necessitating secondary processes like compression molding [19-23].

Several studies have examined plasma treatment's effect on enhancing composite bonding in different polymers. For instance, Li et al. [24] demonstrated a 138% increase in shear bond strength in 3D-printed PEEK/CF after atmospheric plasma treatment. Yildirim et al. [25] observed up to an 84-fold improvement in fracture toughness in CF/PEKK composites after plasma treatment. Jyongsik et al. [26] reported a 52% increase in flexural strength in plasma-

treated CF/PEEK composites. Zhang et al. [27] demonstrated that oxygen plasma treatment of carbon fiber-reinforced epoxy composites reduced the water contact angle from ≈75° to 0°, leading to a 30% improvement in lap shear strength. Similarly, Lu et al. [28] investigated air and argon plasma treatments on CF/PEEK composites, showing a 12.4% increase in interfacial shear strength (IFSS) after 1 minute of air treatment and a 41% increase with argon plasma. These studies underscore the potential of plasma treatments to improve interfacial bonding in high-performance composites.

While prior research has focused on high-melting polymers like PEEK and PEKK, limited studies have investigated plasma treatments on low-melting polyaryletherketone (LMPAEK), especially in the context of ATP manufacturing. No published work, to our knowledge, addresses the air plasma treatment of LMPAEK with carbon fiber in an integrated ATP process, which forms a critical gap in understanding how to optimize in-situ consolidation without secondary processes.

This study aims to bridge that gap by exploring the use of plasma treatment to enhance the interfacial bonding of LMPAEK/CF tapes during in-situ consolidation in ATP manufacturing. Specifically, the objective is to eliminate the need for secondary processes, such as compression molding, by applying plasma treatment directly to LMPAEK/CF UD tapes, which are then processed via ATP. The effectiveness of the plasma treatment is evaluated through various characterization techniques (contact angle, scanning electron microscopy (SEM), X-ray photoelectron spectroscopy (XPS), Atomic force microscopy (AFM)) and performance metrics, including physical, thermal, mechanical, and interfacial properties of the resulting composites.

2. EXPERIMENTAL

2.1 Materials

Low melting Polyaryletherketone (LMPAEK) based UD tape was used to fabricate composites using the ATP system. The ATP hot gas torch head designed and developed by Automated dynamics in 2013 was attached to a Kawasaki ZZX130L 6-axis robot owned by Trelleborg Group, Sweden. The tape comprises a LMPAEK with the melting temperature of 304° C, and a processing temperature of 340° C. The 6.35 mm wide UD tapes were purchased under the trade name of TC1225 LM PAEK/AS4D (34% resin content by weight) (thickness of tape: 0.15 mm), supplied by Toray Advanced Composites, Morgan Hill, CA, USA.

2.1 Plasma Treatment of the UD tape

Plasma treatment is a clean surface treatment, configured using parameters such as treatment time, power, pressure, working gas or carrier gas (depending on its function) - its composition, flow rate, and treatment distance. On the other hand, ATP is a process that lays tape at a specific speed, temperature, and pressure. On the other hand, ATP is a process that lays tape at a certain speed, temperature, and pressure. It was essential to optimize treatment time/speed by keeping the rest of the parameters constant. The air plasma treatment was conducted using Plasma jet (RD1004 Rotary Jet) and generator (FG5001 Openair-Plasma® Generator) supplied by Plasma treat GmbH, Steinhagen, Germany. The plasma jet was kept static with respect to the horizontal plane with a flow rate of 20L/min. The 6.35 mm wide UD tape was passed under the generated plasma, keeping a 12.7 mm distance between the nozzle and tape, as shown in Fig. 1.

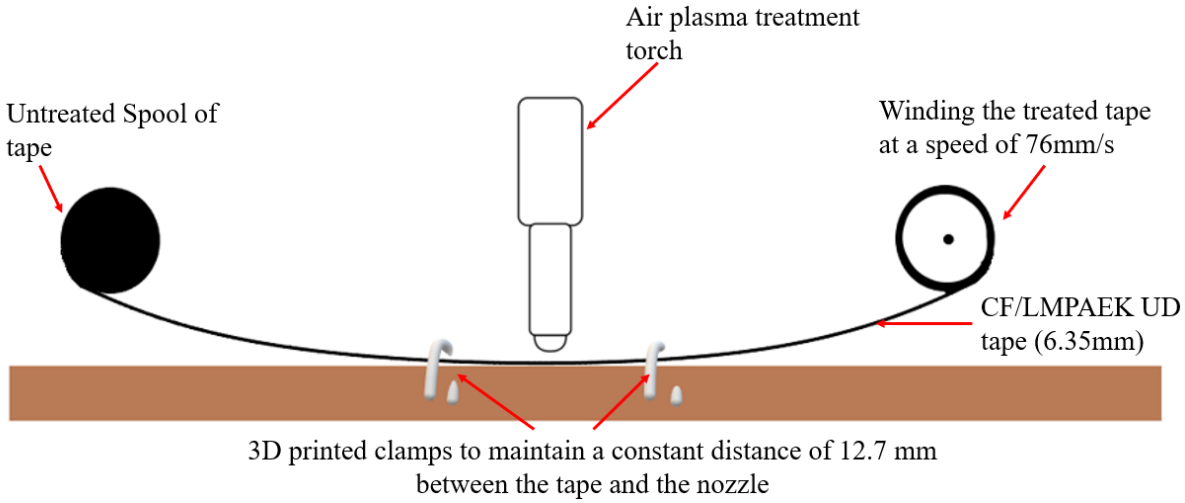

Fig. 1. Illustration of the treatment setup used to treat the LMPAEK/CF UD tape. The tape was treated at the same speed as the deposition rate of the ATP (76 mm/s).

2.2 Development of ATP-based composite laminate.

The composites were developed using the ATP system as shown in Fig. 2. The hot gas torch (HGT) was heated to 840° C (torch temperature) to achieve the nip point temperature of ~ 330° C; a 6.35 mm steel compaction roller with a pressure of 140 N was used, followed by laying 18 layers of UD tape in the one direction (0°) over an aluminium flat mandrel of 1.2 m x 1 m size. The speed of ATP was maintained at 76 mm/s, which was in sync with the speed of the plasma treatment. The composites developed with treated and untreated tape are referred to as C_T and C_U, respectively.

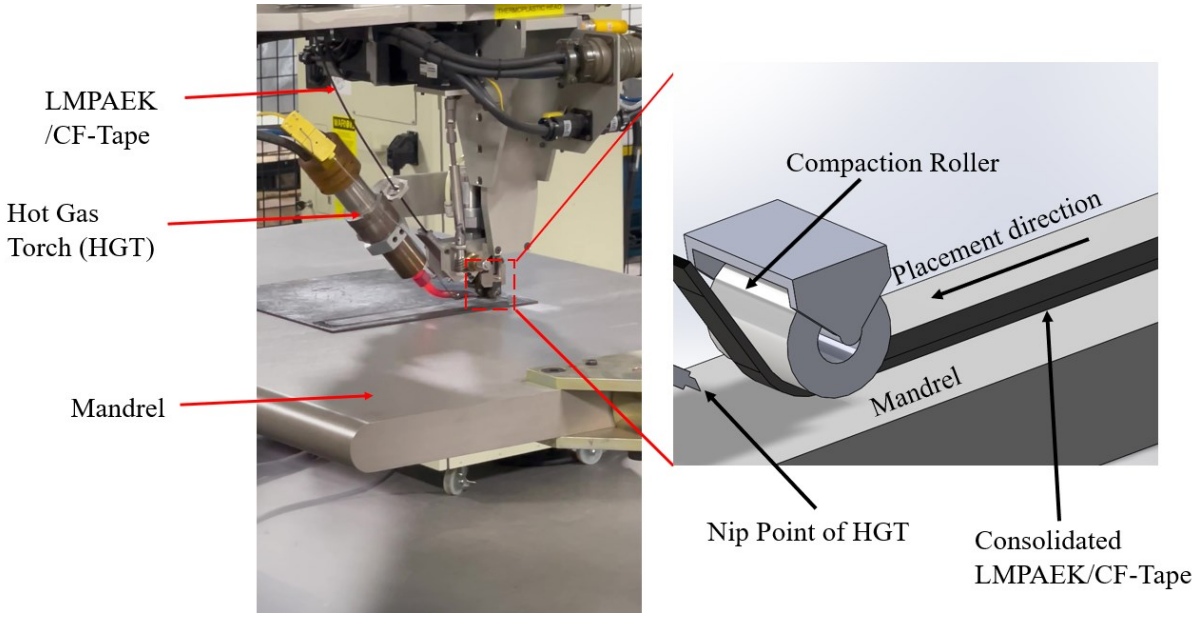

Fig. 2. Schematic depicting the ATP working principle. The LMPAEL CF- tape originates from the feedstock, is subsequently heated by the HGT, and undergoes in-situ consolidation as a specific load is applied through the compaction roller.

2.4 Characterization of LMPAEK/CF UD tape

2.4.1 Contact angle study.

Contact angle studies were performed on treated and untreated tapes using Kruss Goniometer with deionized (DI) water. A drop of 2 µL of DI water (rate of 0.5 µL/s) was placed on the tape sample (6.35 mm x 50.8 mm), 10 samples from different zone of the tape were tested to ensure consistency. Stabilized angles were measured using the ellipse fitting method [29]. Each sample was repeated 8-10 times, and the average values were reported.

2.4.2 Electron microscopy of LMPAEK/CF UD tape

Apart from functional groups, surface treatment (oxidation, plasma, nanoparticle-based treatments) can result in the etching of the carbon fiber surface, thus improving surface roughness [30]. In this study, SEM (Phenom XL G2) was employed to observe the physical changes imparted by plasma treatment to the treated tape. The gold coating was employed to avoid excessive charging and facilitate smoother raster scans.

2.4.3 Fourier Transform Infrared of LMPAEK/CF UD tape

A Fourier Transform Infrared (FTIR) spectrophotometer Vertex-70v was employed for the study. The tape was cut into 6.35 x 6.35 mm and used to collect the FTIR spectra in Transmittance mode. For each sample, 100 scans were recorded in transmittance from 500 to 3500 cm^{-1} wavenumber.

2.4.4 X-ray photoelectron spectroscopy (XPS) surface studies of LMPAEK/CF UD tape

X-ray Photoelectron Spectroscopy (XPS) was utilized to examine the surface of LMPAEK/CF UD tape using a Thermo Scientific K-Alpha X-ray photoelectron spectrometer. This instrument operated in Fixed Transmission Mode with a pass energy set at 200 eV for survey spectra and 50 eV for core-level spectra. It utilized a monochromatic Al Kα radiation source (1486.6 eV) operating at 420 W (14 kV; 30 mA) for incident radiation. Emitted Electrons were collected at a 90° angle from the sample, while maintaining a pressure of around 10^-9 mbar (10^-7 Pa). Six LMPAEK/CF UD tape T and U samples were analysed. One U sample while the other five were T for 5 sec, 10 sec, 15 sec, 30 sec, and 60 sec (named accordingly – T5, T10, T15, T30, and T60). T and U tape samples were attached directly to the XPS sample holder with metal clips followed by spectra acquisition. Shirley background was used for elemental quantification. All measurements were done on the top-middle of tape surface.

2.4.5 Atomic force microscopy (AFM) of LMPAEK/CF UD tape

Cypher AFM (Asylum Research an Oxford Instruments company, Santa Barbara), tabletop system was used in this study. Silicon probes (AC160, OLYMPUS) (tip radius: 7 nm) with an approximate spring constant of 26 N/m and a resonance frequency of around 300 kHz were employed for all AFM measurements. The imaging was conducted in tapping mode within the attractive regime. For processing purposes, all topography images underwent 0^{th} order flattening. The treated and untreated samples were carefully prepared followed by mounting it on carbon tape and subsequently on the AFM stage. 3 samples (6.35 x 6.35 mm) were prepared, and multiple iterations of areal scans were conducted to understand physical, mechanical changes caused by air plasma treatment.

2.5 Characterization of the treated and untreated composites

2.5.1 X-ray diffraction study (XRD)

XRD studies on the treated and untreated composites were evaluated using Empyrean X-ray setup, with a Kα radiation at 30mA and 40kV passing through a ½° divergence slit before interaction with the sample. A set of 5 square samples (20 x 20 mm) were cut off from the laminated composites using a water jet system. The test was conducted at a scan rate of 5°/min for 2Θ varying from 5° to 90°. The XRD data were plotted to find the percentage crystallinity of the tested samples. XRD analysis was performed on LMPAEK/CF UD tape before and after plasma treatment. The crystallinity was calculated with the help of the following equation:

$$\chi_c = \frac{Area\ of\ the\ crystlline\ peaks}{Area\ of\ the\ crystlline\ peaks + Area\ of\ the\ amorphous\ peaks}\ x\ 100 \quad (1)$$

2.5.2 Thermogravimetric analysis

Thermogravimetric analysis (TGA) was performed using a TA instrument. Samples of ~50 mg were placed in a small lead pan while heating was generated with a rate of 10° C/min from 0° to 800°C in the presence of air. Purge gas flow rate to TGA chamber was maintained around ~50 mL/min with nitrogen.

2.5.3 Dynamic mechanical analysis (DMA)

Dynamic mechanical analysis was conducted using TA instruments' QS500. The experiments were conducted from 50°C to 350°C at a ramp rate of 5° C/min at 1 Hz frequency. 2-3 samples with dimensions of 56 x 12 x 2.7 mm (Length x width x thickness) were prepared from each laminated composite in accordance with ASTM D7028 standards. Tests were conducted in three-point bending mode. Storage moduli, loss moduli, and tan delta were recorded as a function of temperature during the experiment.

2.5.4 Interlaminar shear strength (ILSS) study

ILSS tests were conducted in accordance with ASTM D2344. To minimize edge roughness, the specimens were cut using a water jet cutting machine (OMAX 2626, Jet machining center). The tests were conducted in a 3-point bending configuration with a 1.0 mm/min crosshead speed. At least 5 specimens/samples 27 x 5.4 x 2.7 mm (length x width x thickness) were tested to ensure repeatability and statistical relevance.

2.5.5 Flexural strength and modulus study

Test Resources (Model 313 series), Minneapolis, MN, universal testing machine (UTM) with 50 kN load cell was used to perform a three-point bend test of the composites in accordance with ASTM D790. A set of 10 specimens with dimensions of 54 x 12.7 x 2.7 mm (length x width x thickness) of each was produced using the water jet cutting machine. The control rate (0.75mm/min), stress, and strain were calculated based on the test standard.

2.5.6 Tensile strength and modulus study

A set of five specimens was prepared for tensile testing according to ASTM D3039. The average width and length of the tensile coupon were 15 mm and 254 mm, with a thickness of 1.7mm. The test was performed on the 50 kN load cell test resource frame, and samples were pulled at 2 mm/min loading rate. The tensile strain was monitored using an axial extensometer Model 3542, Epsilon Technology Corp, Jackson, WY, USA.

2.5.7 Fractography

201 The failed tensile and ILSS samples were analysed to understand the failure mechanisms. The
202 samples were observed with SEM, QUANT FEG 650.

3 RESULTS

3.1 Characterization of the LMPAEK/CF UD tape

3.1.1 Contact angle study of LMPAEK/CF UD tape.

Fig. 3. illustrates the changes in water contact angle with varying plasma treatment durations. The untreated LMPAEK/CF UD tape initially exhibited a contact angle of 87°, which decreased to 79° after a 5-second plasma treatment. The reduction in contact angle, corresponding to the highest oxygen content (~28%), can be attributed to the saturation of surface functional groups. Once the surface reaches this saturation point, further oxidation has a diminished impact on wettability. Additionally, increased oxygen concentration may alter surface morphology, such as introducing micro-roughness, which limits further reductions in the contact angle. This behavior is consistent with prior studies showing that beyond a certain threshold, further oxidation yields diminishing returns in wettability improvements [31].

As the treatment time extended to 10, 15, 30, and 60 seconds, the contact angle further dropped to 24° and 22°, then increased to 36° and 37°, respectively. The rise in contact angle after extended plasma exposure is likely due to increased nano-scale surface roughness, which is known to affect wetting behavior [32]. The overall decrease in contact angle reflects an increase in surface free energy and the development of hydrophilic functional groups on the tape's surface, indicative of oxidation.

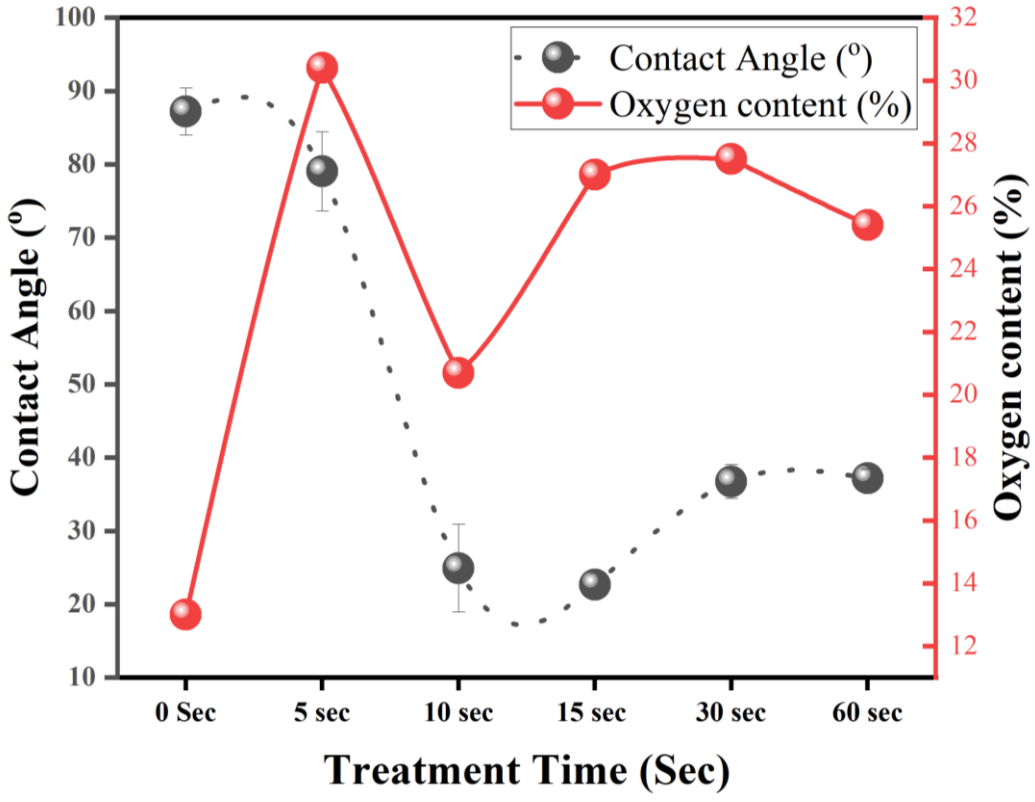

Fig. 3. The contact angle for treated tape as a function of treatment time: With the increase in plasma treatment time, the contact angle reduced drastically. Additionally, with the increase in contact angle after 15 sec treatment time, it increases again due to an excessive increase in surface roughness [33]. The right Y axis shows the increase in oxygen content on the surface (analysed from XPS spectra), i.e., polarity with treatment time. An increase in oxygen content on the treated tape surface was found to be nonlinear with treatment time, however, demonstrates the effectiveness of treatment.

Fig. 4 depicts the contact angle photographs for treated and untreated samples. In the case of Fig. 4a (untreated sample), the contact angle was 87° due to borderline hydrophobicity on CM/LMPAEK tape caused by the lack of hydrophilic moieties on LM-PAEK. With treatment, the contact angle reduced to 22°, as seen in Fig. 4b. The fall in contact angle for treated tape is supported by XPS and FTIR data. Increase in concentration of hydrophilic moieties and oxygen content demonstrated by FTIR and change in % oxygen content through XPS in subsequent sections.

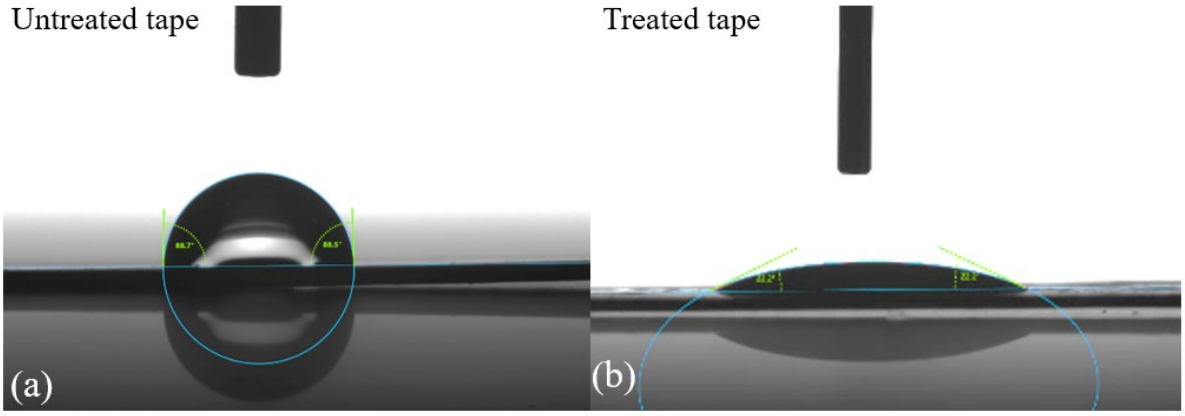

Fig. 4. Contact angle measurement optical image plasma untreated tape (a) and the treated tape (b). Reduced contact angle post plasma treatment is effect of formation of hydrophilic moieties on the surface of ATP tape, cleaner surface.

3.1.2 FTIR analyses on the LMPAEK/CF UD tape

LMPAEK is a semicrystalline thermoplastic polymer characterized by the Phenylene rings (R-rings) attached to ether, carbonyl and ketone via oxygen bridges (O) as shown in Fig. 5. During air plasma treatment, oxygen and nitrogen-based reactive species activates the surface of the media [34].

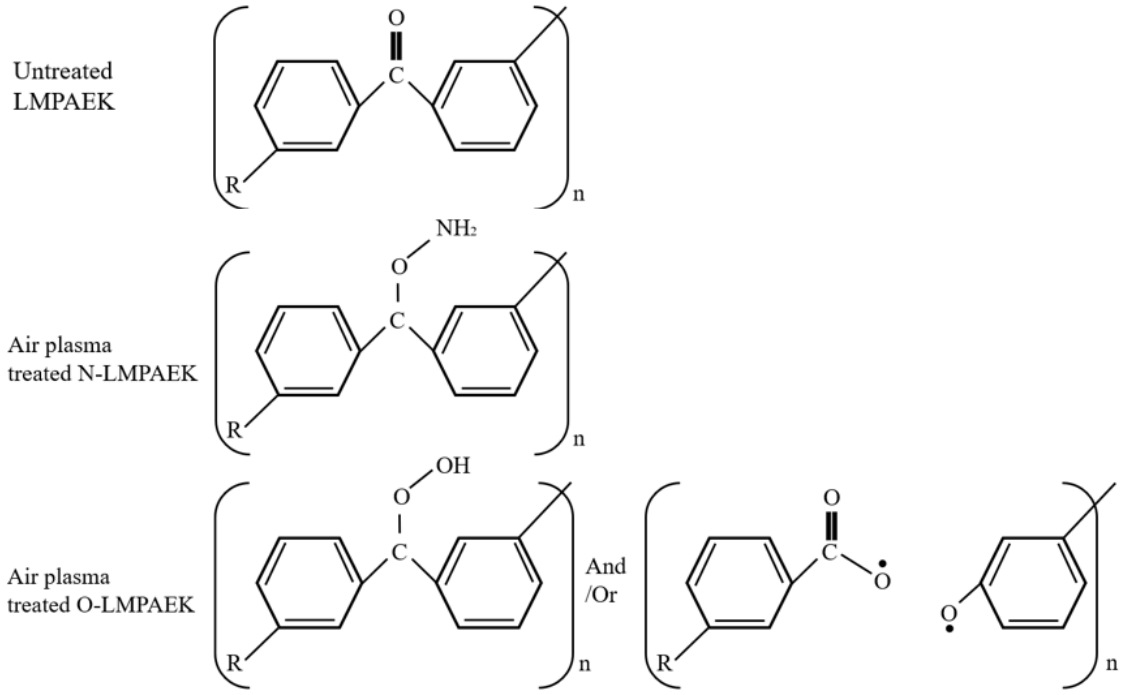

Fig. 5. Possible chemical changes of LMPAEK/CF UD tape due to air plasma treatment [35, 36].

Fu et al [35] reported the possible chemical groups occurred during H-plasma and O-plasma treatment of PEEK, same family as LMPAEK. Based on their study and on the literature, it could be assumed that during the air plasma treatment the C=O bond may have been converted into C-O-OH, O-C=O in case of Oxygen and/or C-O-NH_2 by plasma-reactions from Oxygen and Nitrogen plasma-species as shown in Fig. 5. FTIR studies were conducted on the treated (T) and untreated (U) LMPAEK/CF UD tape to understand the chemical functional group variation of the tape (Fig. *6*). The peaks observed in the range from 3000 cm^{-1} to 3150 cm^{-1} in the T tape were assigned to O-H functional group due to plasma treatment in comparison with the U tape. The peaks ranging from 2650 cm^{-1} to 2750 cm^{-1} shows the presence of the C-H and C-O stretch and it can be noticed that the intensity of the peaks in the T tape is higher than the U one. The existence of the C-H/O stretch with low intensity in the U tape could be related to the presence of phenyl group (C_6H_5-). (Carboxyl group (C-O stretched) could be observed as well in the range between 1450 cm^{-1} and 1750 cm^{-1} with stronger peaks intensity in the T tape compared to U. An intense peak was observed between 2160 and 2250 cm^{-1} in the absorbance sector that could be referred C≡C or C≡N. The increased intensity of the polar functional groups, in the plasma treated samples can enhance the bonding interactions with the adjacent

tape through mechanisms such as covalent and hydrogen bonding, resulting in improved adhesion and mechanical properties [37, 38].

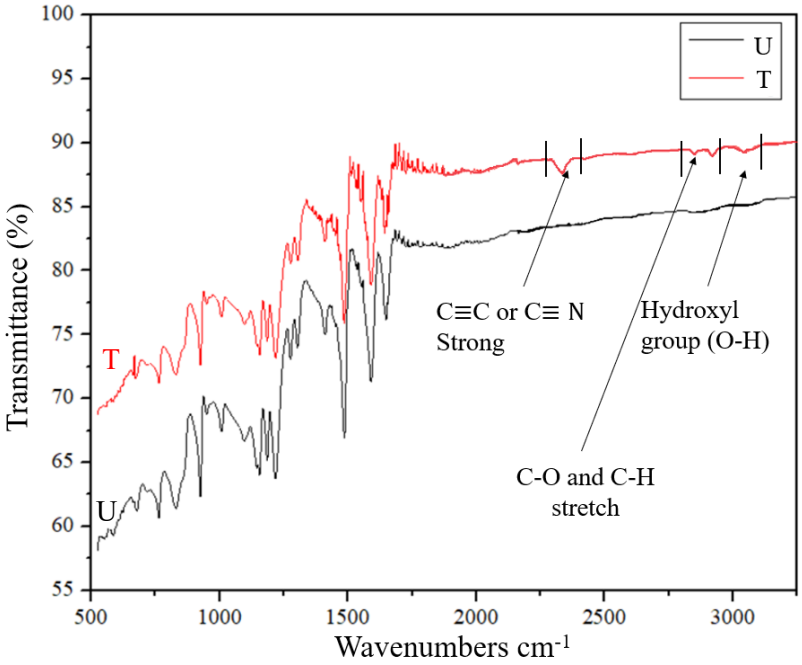

Fig. 6. FTIR spectrum of the LMPAEK/CF UD treated and untreated tape. Appearance of a new peaks between 2160 and 2250 Cm^{-1}. The intensity of the hydroxylic group and C-O stretch and C-H stretch are higher in the T tape compared to U.

3.1.3 XPS surface studies of LMPAEK/CF UD tape.

A wide binding energy range survey spectrum was acquired on each sample to identify all elements present. A set of narrow energy range core level spectra were acquired for each identified element. A second set of data (survey and core level spectra) were acquired at a different area of each sample to gain some insight into the surface uniformity. Fig. 7 shows the overall surface composition of each sample. High resolution spectra result further corroborated the data from FTIR and contact angle wettability studies, indicating more oxygen bonded carbons (C-O and O-C=O) on the surface than C-C bonds due to air plasma processing.

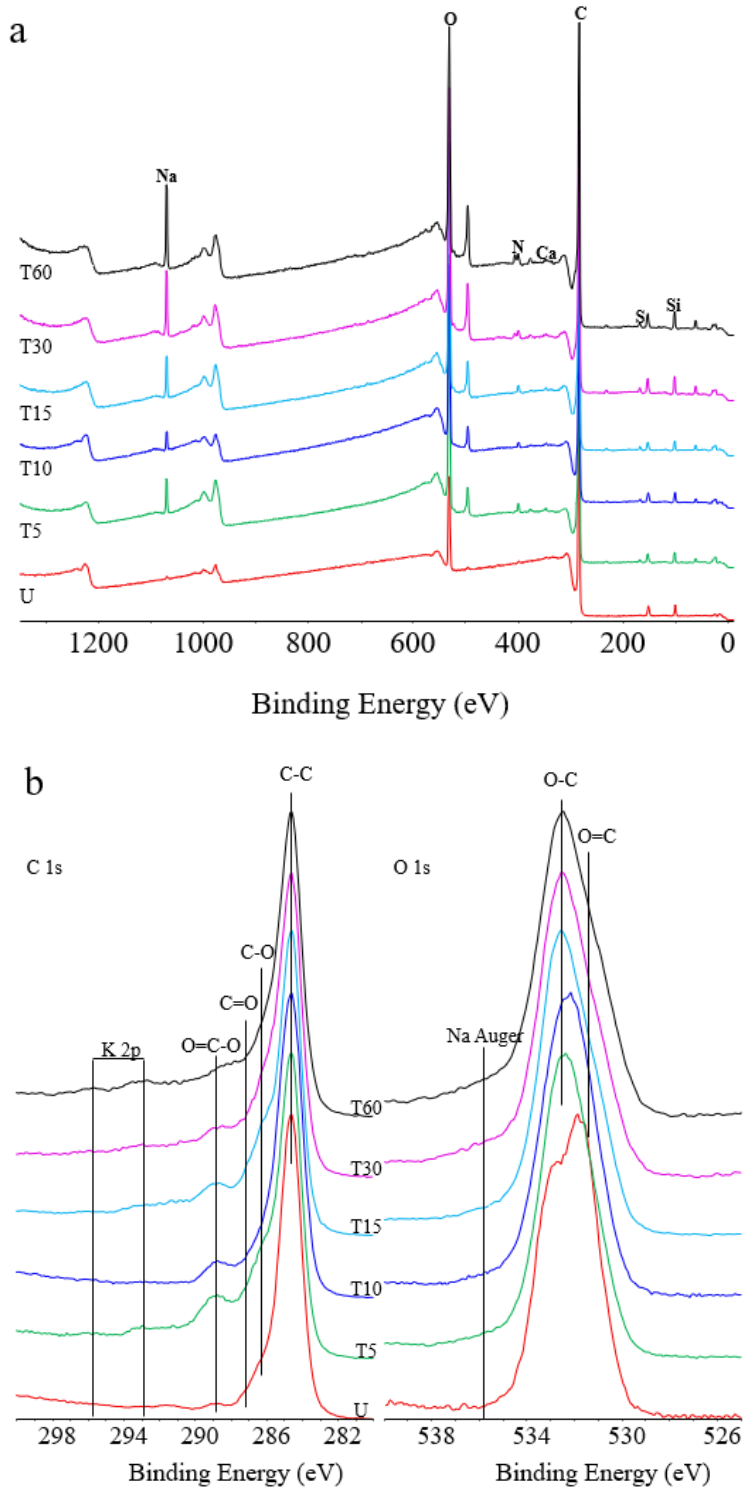

278

279

280 Fig. 7. XPS survey spectrum (a) for the U and T LMPAEK/CF UD tape. The peaks intensity
281 of Oxygen (O) and Nitrogen (N) are higher in the T samples compared to the U emphasizing
282 the effect of plasma treatment on the surface. (b) deconvoluted XPS spectra for C 1s and O
283 1s.

284 The amount of carbon (C) for the sample U i.e. untreated tape was highest. With treatment, the
285 C content decreased, and oxygen (O) content improved. The increase in O content depicts the
286 oxidation imparted by the plasma on the tape surface. The O increased from 13 at. % for the

tape U to above 25 at. % for the tape T sample (Tape T-5sec) showed highest oxygen content of 30 at. %, the 5 sec treatment equivalents to with typical ATP layup speed (76mm/sec), N also increased for each of the T samples (~1-3 at. %) as compared to the U sample as shown Table 1.

Table 1. Surface Composition (at.%) for the U and T LMPAEK/CF UD tape for element C,O and N.

	C	O	N
U	82.8	13.0	0.6
T5	62.1	30.4	1.7
T10	73.9	20.7	0.9
T15	66.1	27.0	1.4
T30	61.3	27.5	2.3
T60	62.7	25.4	2.9

3.1.4 Microscopy Studies of LMPAEK/CF UD tape

Surface treatment oxidizes the carbon fiber surface through different oxidation mechanisms, introducing a range of functionalities, both chemical and physical, on the surface of carbon fibers [15]. Physical functionalities may include creating a rougher surface and increase surface area, which can improve mechanical interlocking between the fiber and matrix, and remove weaker regions from the fiber surface [15]. In the current study, the change in surface was qualitatively studied using SEM. Fig. 8 depicts the SEM micrographs for untreated (a) and plasma-treated (b) tape.

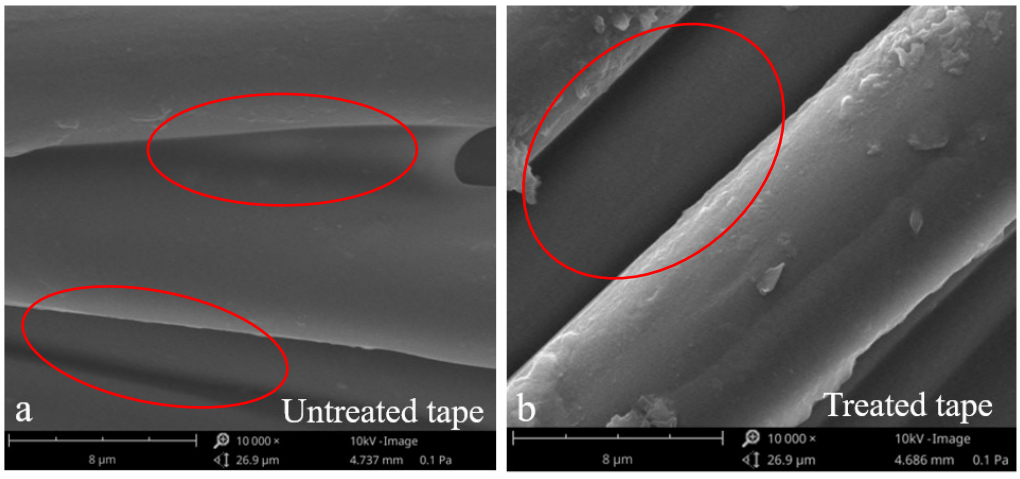

Fig. 8. SEM micrographs for U (a) and T (b) LMPAEK/CF UD tape: SEM micrographs depict nature of attack of plasma species. U (untreated tape) tape depicts uniform and coherent surface

with no surface damage, whereas the plasma treated tape shows vivid feature i.e., increased surface roughness, deeper crevices, and blistering of LMPAEK in the T (treated tape) tape.

It is evident from Fig. 8(a) that untreated tape possesses a smooth surface and no defect or physical etching. In the case of Fig. *8*(b) i.e., for treated tape, surface roughness was observed, resulting from the interaction of polymeric surface of tape with ionic species and free radicals during plasma treatment [1].

3.1.5 Atomic force microscopy (AFM) of LMPAEK/CF UD tape

Fig. *9* presents surface topology images obtained via Atomic Force Microscopy (AFM), comparing the surface topography of plasma-treated and untreated samples within both fiber-rich and polymer-rich regions. Observations from fiber-rich regions, Fig. 9a and b, highlight inter-fiber crevices, appearing as deep valleys. Substantial variation in inter-fiber crevices has been observed across the entirety of both samples which hampered direct quantitate evaluation of surface roughness in these regions. However, simple qualitative analysis reveals that the fiber surfaces are smoother in untreated samples, a finding corroborated by SEM observations in section 3.1.4. However, as mentioned the significant height disparities and curved surface across fibrous areas hindered accurate quantitative assessment of surface roughness. Further measurements in the flat areas have been conducted, polymer-rich regions situated between the fibrous areas. Fig. 9(c, d) presents 2D height images for untreated and treated samples, specifically targeting these polymer-rich regions. Utilizing a grayscale across all images facilitates an immediate and clear comparison, illustrating a noticeable increase in surface roughness following plasma treatment. Quantitative analysis of the root means square roughness indicated a more than twofold increase, from 320 pm to 820 pm standard deviation, between untreated to treated samples respectively. The relatively smoother surfaces of these polymer-rich regions enabled the determination that the treated samples exhibit distinct surface features, a direct result of the interaction between mixed ionic species and the LMPAEK surface. Surface roughening increases the effective bonding area, improves the surface area for convective heat transfer between heated N_2 gas and LM-PAEK/CF tape, improving mechanical interlocking between the tape and substrate. This enhanced interaction leads to better consolidation during the ATP process.

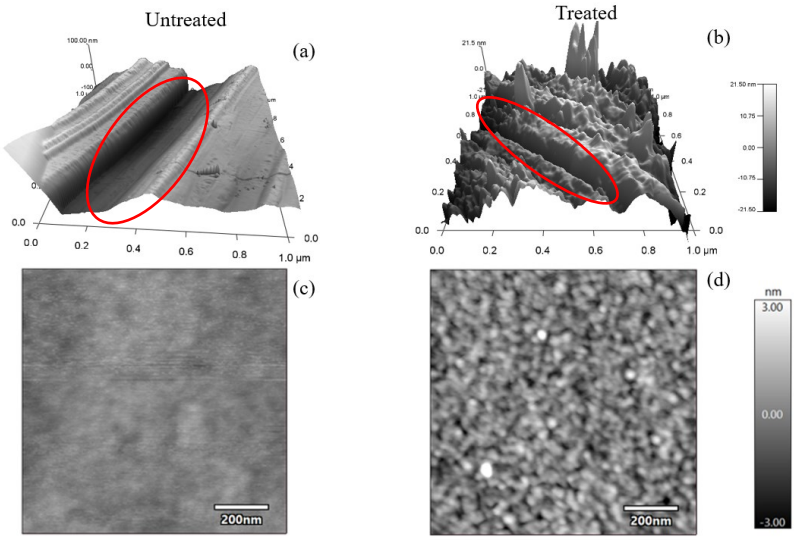

Fig. 9. Comparative AFM topography imaging of LMPAEK/CF UD tape for both untreated (a, c) vs. treated (b, d) samples. Panels (a) and (b) depict 3D topography focusing on fiber-rich regions. Panels (c) and (d) are 2d images for polymer rich regions, illustrating changes in surface structure post-treatment.

Interaction of plasma species with polymer could result in change in chemical, physical and mechanical properties of surface through different mechanisms such as micro-etching, cleaning of organic contamination and chain scission vis-a-vis polymer degradation [38]. The AFM profile obtained in this study suggests micro-etching and chain scission as active mechanism. The dominant effect usually depends upon operating parameters of plasma treatment and determines extent of surface functionalization, crosslinking and degradation [39, 40]. For treated sample, it was observed that there was change in the surface roughness, and it was effect of surface cleaning i.e. removal of surface adsorbed contamination, degradation of low molecular weight moieties and polymer chain scission on carbon fiber rich and polymer rich area, which could create further low molecular weight polymer surface layer [41]. Fig. 10a shows untreated tape's polymer rich region depicts relatively uniform surface and change in roughness over the region, whereas Fig. 10b illustrates wide variation in roughness across the

region depicting the polymer surface etching achieved by plasma treatment. The Grayscale on the right of 2D profiles portrays the extent of difference in the Z axis variation.

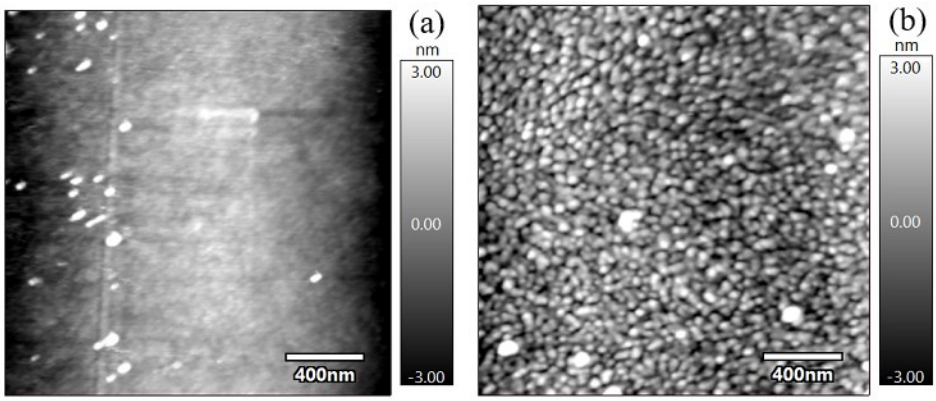

Fig. 10. 2D profile of polymer rich region of untreated (a) and treated (b) LMPAEK/CF UD Tape by AFM.

3.2 Characterization of treated and untreated composites

3.2.1 Thermogravimetric analysis

Fig. 11 illustrates the results of thermogravimetric analysis for both treated and untreated tapes, revealing only a slight modification in thermal degradation behaviour. Table 2 presents the temperatures at which 5% (T5) and 10% (T10) weight losses occur for the developed composites. The untreated composite labelled C_U exhibits marginally lower T5 and T10 temperatures in comparison to its counterpart, C_T. This increased weight loss observed in both composites can likely be ascribed to enhanced oxidation, a consequence of exposure to an air environment. The residue percentage has been considered at 800°C, the residue percentage of C_U (8.79%) was lower than C_T (16.40%). Similar thermograms (Fig. 11) for developed composites shows that plasma treatment did not lead CF-LMPAEK tape to thermal mass degradation.

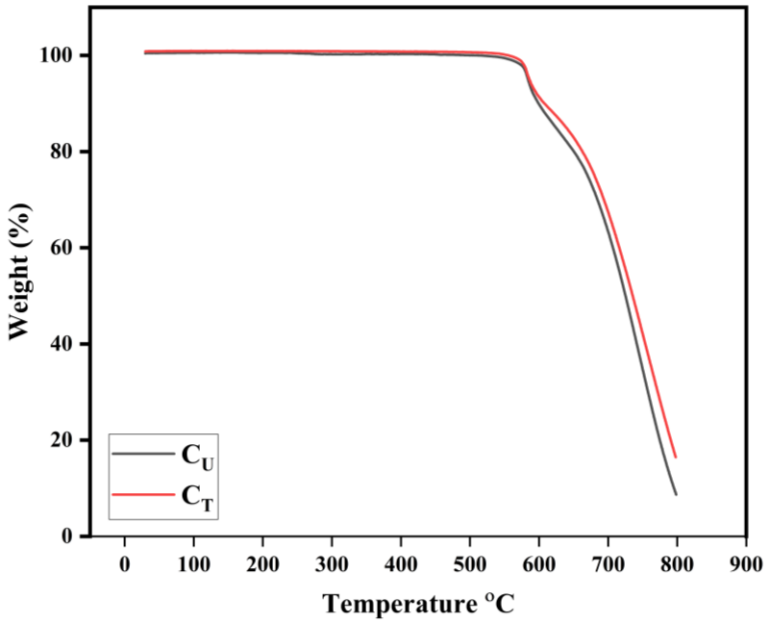

Fig. 11. Thermogravimetric analysis for composite C_U and C_T

Table 2. T5 and T10 temperatures for composite C_U and C_T

Composites	T5 (° C)	T10 (° C)
C_U	583.79	598.62
C_T	586.33	609.18

3.2.2 Dynamic mechanical analysis (DMA)

Fig. 12 illustrates the variations in (a) the storage modulus (E') across a specified temperature spectrum (50-275° C), and (b) presents the tan δ values. Concurrently, Table 3 shows the storage modulus metrics at 50° C alongside the glass transition temperatures for C_U and C_T. Fig. 12 in conjunction with Table 3 elucidates that the composite material C_T exhibits a superior storage modulus at 50° C when compared with C_U. This improvement in storage modulus is attributable to the enhanced interlaminar adhesion facilitated by the synergistic effect induced by chemical and physical modifications achieved through the plasma treatment employed on the LMPAEK/CF UD tape before tape layup using ATP system. Chemical and physical modification observed due to plasma treatment corroborates with the mechanical response of composite C_T under tensile stress, where composite C_T demonstrates a failure mode characterized by singular point fracture as opposed to the multi-layered delamination observed in C_U load-displacement behaviour as depicted in Fig. 15, Fig. *17*). Furthermore, C_T shows an elevated glass transition temperature relative to C_U indicating a marginal increment, which is an indicator of the enhanced inter-ply and interfacial interactions within C_T composites at molecules scale. Added chemical functionality (hydroxyl and carboxyl groups) by plasma

treatment on CF/LMPAEK tape results in covalent and/or secondary bonding between treated CF/LMPAEK tape and substrate tape (exposing untreated side) [42]. The chemical interaction was found to be at the polymer-polymer (of two adjacent tapes) interface (explained in section 4) and not at the polymer-fiber interface. This improved molecular interaction (which is lacking in the conventional ATP process) results in improved yet comparable mechanical performance (tensile and flexural strength and their failure modes).

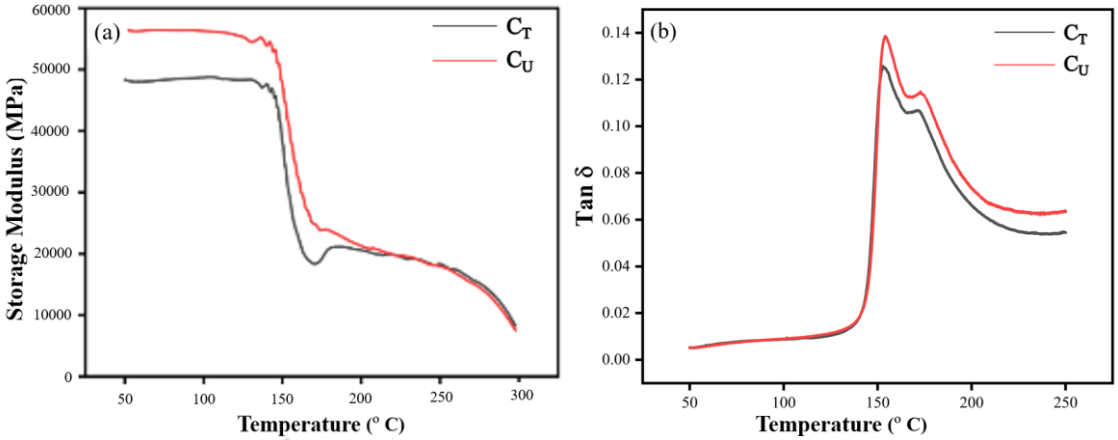

Fig. 12. Visco-elastic performance of developed composites (a) storage modulus and (b) tan δ.

Table 3. Storage moduli and glass transition temperature by dynamic mechanical analysis

Properties	**C_U**	**C_T**
E' at 50° C (GPa)	48.33	56.71
T_g (° C)	152.75	154.90

3.2.3 Crystallinity measurement of C_T and C_U.

The crystallinity values for C_U and C_T were 29.4 and 33.2 %. The crystallinity is directly affected by the cooling rate applied on the tape during manufacturing [21] .However, in this study both C_U and C_T were processed with identical parameters. The findings that the crystallinity of C_T was higher than C_U could be due to the effect of air plasma treatment on the LMPAEK/CF UD tape. Korycki et al [43] mentioned in their studies that the crystallinity of the materials would be affected by plasma treatment. However, achieving a higher crystallinity would increase the shear strength, tensile strength and modulus of the composites [21, 44].

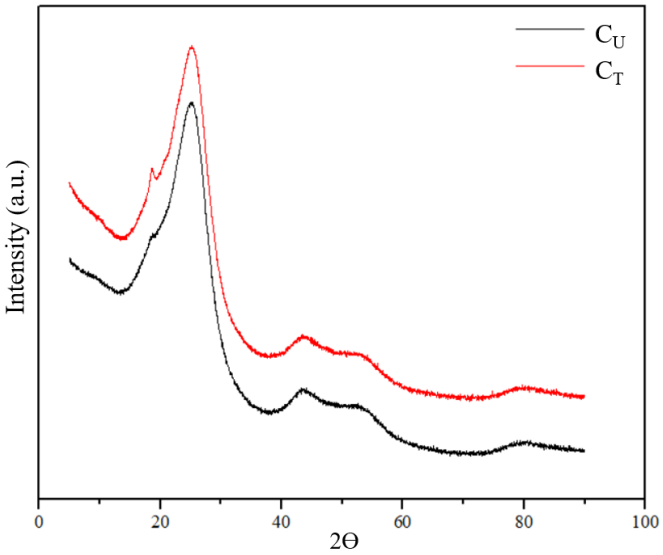

Figure 13. X-ray diffractogram for the developed composites C_T and C_U.

3.2.4 Interlaminar shear strength (ILSS)

Fig. 14a shows the ILSS behavior of the C_U and C_T. ILSS of C_T improved by ~ 18% compared to C_U. The improvement in ILSS samples can be attributed to the effect of air plasma treatment on the LMPAEK/CF UD tape. The increase of surface energy witnessed by contact angle (87° to 22°) and the increase of the surface roughness monitored by AFM, alongside the formation of hydroxyl/carboxyl group reported by FTIR, led to a higher ILSS in C_T than C_U. The air plasma treatment influenced the failure mechanism of C_T as well. Fig. *15* shows the failure analysis of the C_U and C_T tested samples. It was observed that delamination occurred in both ILSS tested samples (C_U and C_T). Fig. 15a showed that the samples extracted from the C_T exhibited a single time failure. However, the samples tested from C_U displayed a multiple crack in the sample before attaining the complete failure as shown in Fig. 15b. This behavior is also reflected in (Fig. *14*b) where C_U demonstrates non-linear behavior, with progressive failure and delamination, while C_T exhibits a single failure after reaching maximum load, characterized by a more linear response prior to the attaining the maximum.

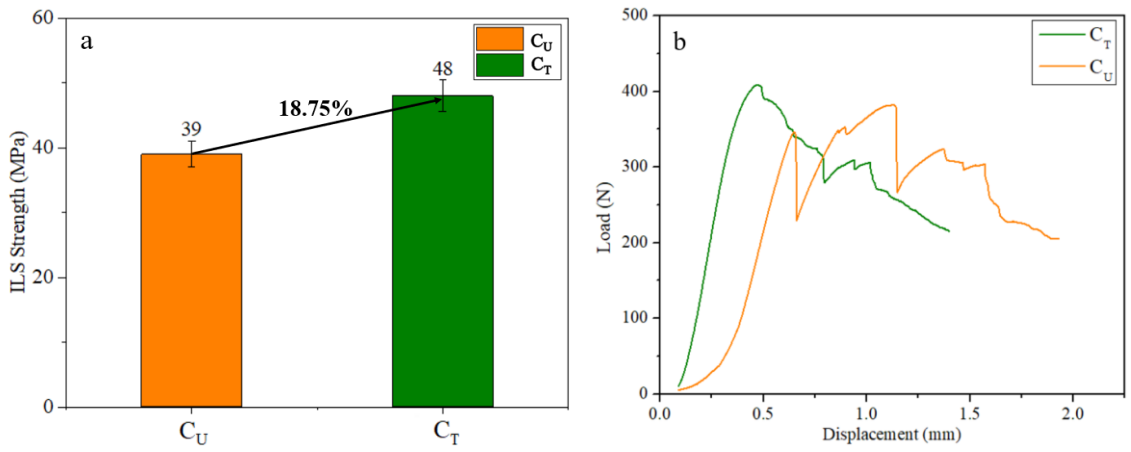

Fig. 14 (a, b). Average interlaminar shear strength of the C_T and C_U. An enhancement of 18.75% has been noticed in the C_T compared to C_U. Load vs displacement depicting the failure behavior of the ILSS samples.

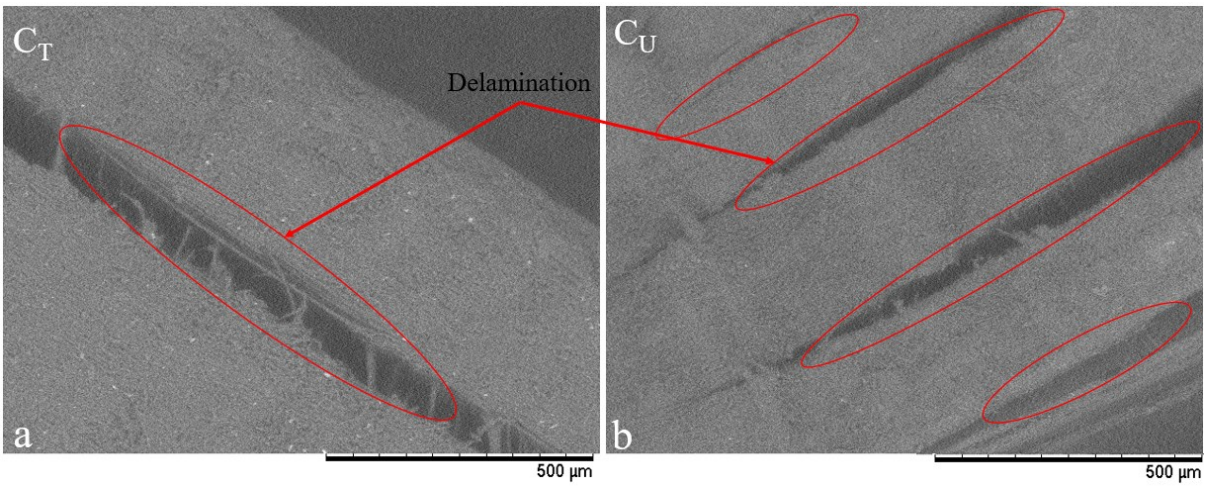

Fig. 15. (a, b). SEM images of failed ILSS samples of C_T and C_U respectively. Delamination was observed almost between each laminate in the C_U, and just in one spot for the C_T.

3.2.5 Flexural Strength and Modulus

Air plasma treatment of the LMPAEK/CF UD tape affected the flexural behavior of C_T and C_U. It was noticed that the flexural strength and modulus of C_T were approximately 18% and 8.3% higher than the C_U, respectively, as shown in Fig. 16a. Along the flexural properties enhancement, a different failure behavior between C_U and C_T samples was observed. Fig. 17(a, b) illustrate low-magnification optical microscopy (OM) images for the tested flexural specimens. It was perceived that the coupons extracted from the C_T exhibited a failure in tension according with ASTM D790. The flexural tested samples of C_U displayed a delamination along the length coupons. In the case of composite C_U, the major failure mechanism includes inter-laminar delamination caused by weak inter-tape adhesion. On the other hand, post treatment-composite C_T, the dominating failure mechanism shifts to fiber breakage, matrix cracking on (tension dominated) bottom side of flexural specimen. This behavior is also evident in (Fig. *16*b) where C_U exhibits progressive failure and delamination, while C_T demonstrates a typical failure pattern characterized by an initial linear response up to the ultimate strength, followed by a transition into a plastic deformation zone and final failure in tension. Fig. 17(a, b) demonstrates that the plasma treatment reduces the inter-tape delamination (inferior performance) and increased interlaminar adhesion. The matrix failure and fiber breakage were observed as the dominating failure mechanism for composite C_T.

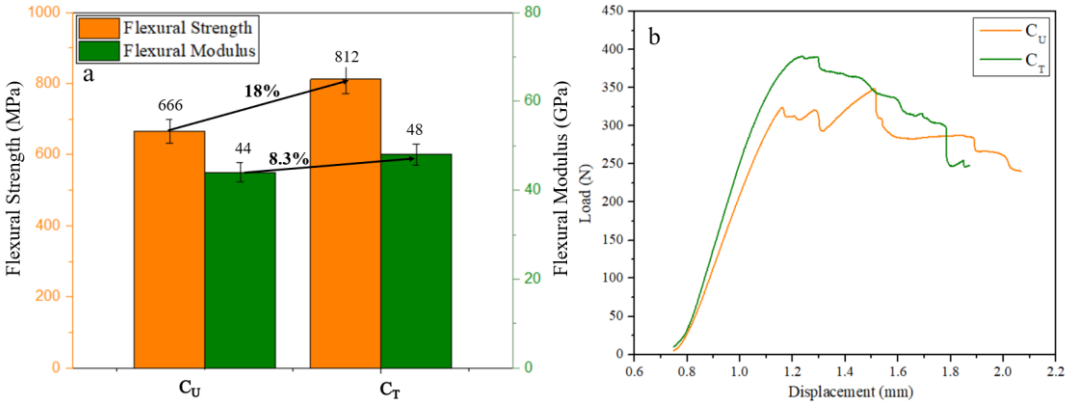

Fig. 16 (a,b). Average flexural strength and modulus of C_T and C_U in accordance with ASTM D790. The flexural strength and modulus of C_T is 18% and 8.3% higher than C_U. Load vs displacement depicting the failure behavior of the flexural samples.

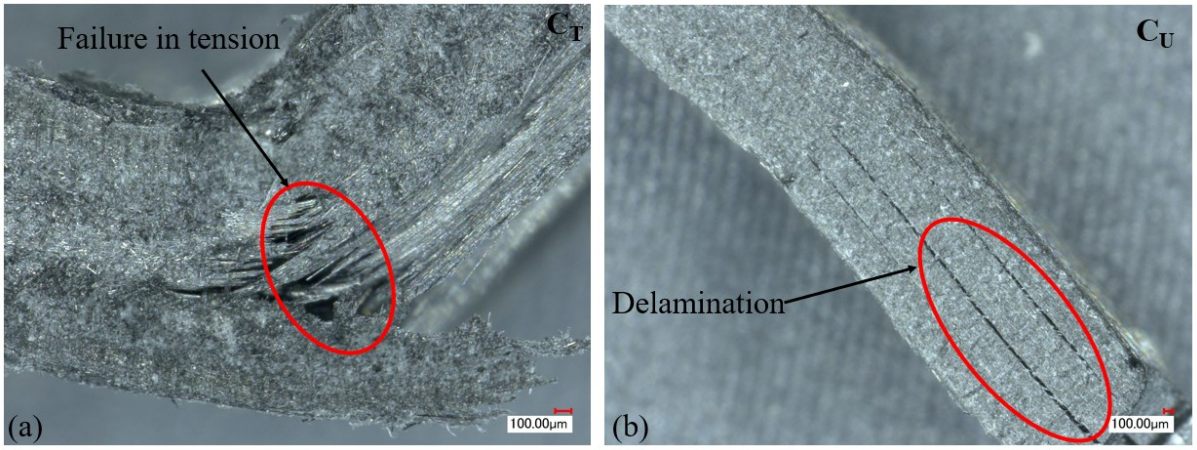

Fig. 17(a, b). Optical microscopy (OM) images show ASTM D790 acceptable failure behavior for the C_T, brittle failure mode in tension, and interlaminar failure mode in the C_U specimens, illustrating delamination in the samples.

3.2.6 Tensile Strength and Modulus

Air plasma treatment had a positive impact on the tensile behavior of C_T. Fig. 18a shows the average tensile strength and modulus of the C_T and the C_U. An improvement of 7.6% has been noticed in the tensile strength, with 8% in the tensile modulus, as shown in Fig. 18a. The load versus displacement behavior of two C_U and C_T samples have been reported as seen in Fig. 18b; The failure mechanism showed that the C_U samples attained several cycles of maximum/minimum load before approaching a complete failure at ~25kN with a displacement of 18.5 mm, elucidating delamination, and fiber debonding behavior. The outcome of plasma treatment was noticed in the failure behavior of the C_T samples, the linearity, and the brittle failure, as shown in Fig. 18b.

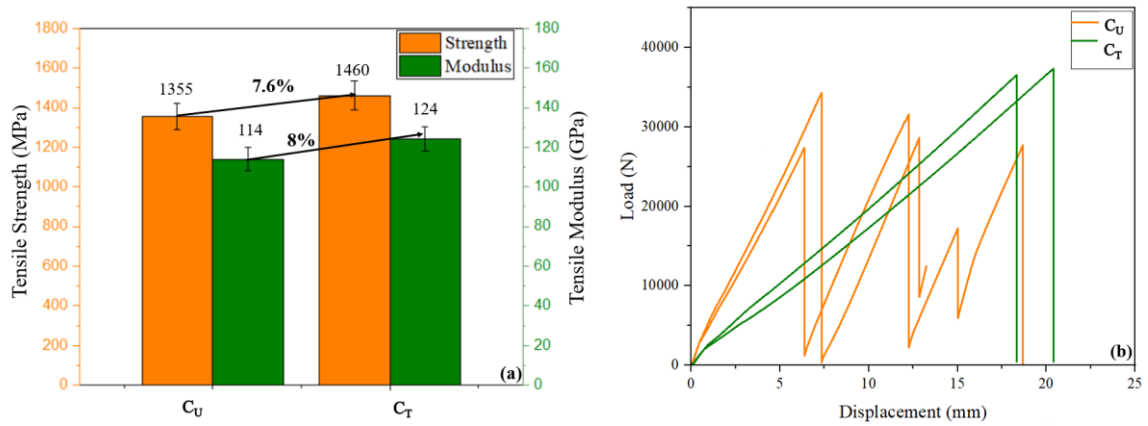

Fig. 18a. Average tensile strength and modulus for C_T and C_U. An increase of 7.6% in strength and 8% in modulus has been noticed in the C_T. Fig. 18b shows load versus displacement, illustrating the failure behavior of the tensile samples.

3.2.7 Fractography

Fig. 19 shows the SEM micrographs for the failed samples under tensile loading. Fiber matrix debonding was the primary failure mechanism for the C_U variant. Deboned fibers and cavities of carbon fibers are marked in Fig. *19*a. The failure of carbon fiber was brittle in nature for both composites, which is consistent with the literature [8, 45, 46]. In the case of C_T, the absence of fiber matrix debonding, as shown in Fig. *19*, depicts that the plasma treatment activates the surface by imparting chemical and physical attributes to the ATP feedstock tape, resulting in stronger bonding between carbon fiber and LMPAEK, which is reflected in mechanical properties evaluation and interlaminar shear strength performance (Fig. 16,Fig. *17* and Fig. *18*).

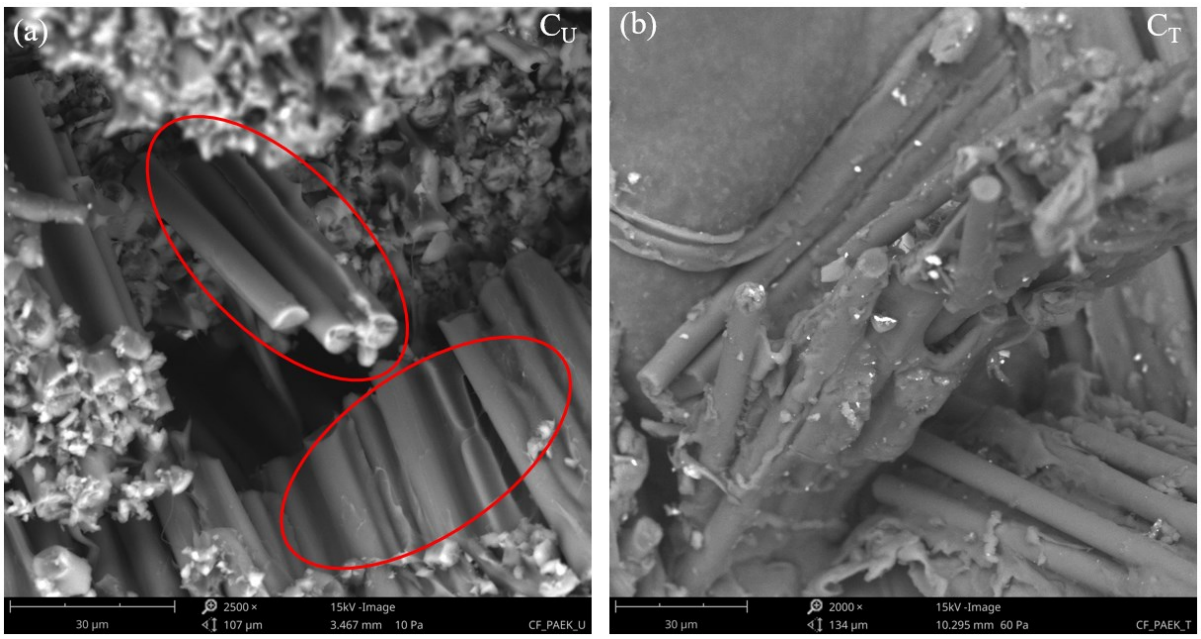

Fig. 19. SEM micrographs depicting failed samples during tensile test (a) C_U and (b) C_T.

4. DISCUSSION

Different characterizations, such as contact angle measurements, FTIR, and AFM, were conducted to investigate the effect of plasma treatment on the surface of LMPAEK/CF UD tape. In the case of water contact angle measurement, it was observed that the contact angle decreased to 22° from 87°. The decrease in contact angle indirectly suggests that the surface was more receptive to polar interactions due to the formation of chemical functional groups. The increased presence of functional groups was confirmed by FTIR spectra. These polar groups were introduced through the reactive species (from plasma treatment) with the polymer chain, resulting in the formation of ketone group, peroxide-carbonyl, and hydroxyl groups on the PAEK, the functional groups interact with each other covalently (forming strong interaction between hydroxyl and carboxyl groups) or through van der waal forces such as hydrogen bonding (especially in the case of amine functional groups). These chemical interactions result in strong LMPAEK – LMPAEK interactions. Alongside chemical modification, plasma treatment imparts a certain roughness to the CF/LMPAEK surface. AFM measurements demonstrate the change in surface roughness/topology for plasma-treated LMPAEK/CF UD tape. Polymer chain scission (potential) and etching (proved through AFM experiments (section 3.1.5)) are the foremost mechanisms that contribute to increased surface roughness, as supported by current study and prior research. Applying controlled roughness through surface treatment can enhance the mechanical bonding between substrates (in the current study CF/LMPAEK UD tape). However, excessive roughness of both the polymer and reinforcement could lead to a decline in composite properties due to defects introduced during the surface treatment process [38, 47].

The effect of plasma treatment increased surface roughness vis-à-vis surface area for plasma treated LMPAEK/CF UD tape results in more efficient melting/softening (efficient heat transfer due to enhanced surface area) of the ATP tape compared to untreated tape. Furthermore, the chain scission, degradation of low molecular weight chains, and physical surface defects (such as surface damage at (nanoscopic/microscopic level) and contamination on LM-PAEK/CF ATP tape - majorly originated from handling of tapes) removal due to plasma treatment, can result in relatively low defect, improving interaction between two adjacent tapes. Beyond better homogeneity, the functional groups extend covalent bonding between tapes. These chemical and physical interactions were evident in the improvements in ILSS (18.75%), flexural strength and modulus (18% and 8.3%), and tensile strength and modulus (7.6% and 8%) properties in C_T compared to C_U, respectively. The absence of delamination during mechanical testing

captured by OM and SEM (in failed samples) demonstrated the interlaminar homogeneity for C_T.

CONCLUSIONS

The study investigates the integration of continuous plasma treatment in the ATP process to enhance the production of ATP-based composites with superior properties. Air plasma treatment was shown to be an effective way to enhance the in-situ consolidation of LMPAEK/CF UD tape processed through HGT on the ATP. It involves the treatment of LMPAEK/CF UD tape at a specific ATP feed rate. Key findings include:

- The air plasma treatment not only enhanced the surface characteristics of the LMPAEK/CF UD tape, leading to improved adhesion and interfacial bonding, but also demonstrated compatibility with the ATP process without introducing any defects.
- The treated tape showed a fall in water contact angle by ~65°, which corresponds to the formation of hydrophilic chemical functional groups. The change in the roughness of LMPAEK/CF UD tape corroborates to physical changes caused by plasma treatment.
- The composite C_T (developed from treated tape) shows improved tensile strength and modulus, flexural strength and modulus, and ILSS by 18.75%, 18% and 8.3% and 7.6% and 8%, respectively.
- The primary mechanisms behind these enhancements include the development of chemical functionality and subsequent covalent bonding and hydrogen bonding to the overlapping tape while processing, improved surface roughness due to plasma treatment, and the removal or degradation of surface imperfections from the LMPAEK/CF UD tape surface.
- The failure mechanism for the short beam test for ILSS was changed from inter-ply delamination to matrix cracking, fiber pull out, fiber pull out and matrix cracking.

ACKNOWLEDGEMENT

The authors acknowledge the support from the US Department of Energy (DOE), Office of Energy Efficiency and Renewable Energy, and Advanced Materials and Manufacturing Office. http://energy.gov/dow nloads/doe-public-access-planThe authors extend their gratitude to Chase McCullar for his assistance in carrying out mechanical testing. Additionally, they wish to thank SEAMTN (HQ00052110069) for providing resources for the tape cut and surface

analysis, Institute of Advanced Composites Manufacturing Innovation (IACMI) (DE-EE0006926) for granting access to the ATP robot and other assets, Plasmatreat north America for providing the air plasma setup, and IUCRC (A22-0196) for offering technical assistance and resources.

REFERENCES

[1] Marathe UN, Bijwe J. High performance polymer composites - Influence of processing technique on the fiber length and performance properties. Wear. 2020;446-447.
[2] Sahu R, Ponnusami SA, Weimer C, Harursampath D. Interface engineering of carbon fiber composites using CNT: A review. Polymer Composites. 2023.
[3] Simaafrookhteh S, Tsokanas P, Loutas T, Lomov SV, Ivens J. Measuring the interlaminar fracture toughness of thin carbon fiber/polyamide6 composites using adhesively bonded stiffeners. Composites Part A: Applied Science and Manufacturing. 2023:107841.
[4] Wasti S, Schwartz B, Yeole P, Chahine G, Tekinalp H, Ozcan S, et al. BAMBOO FIBER Overmolding Textile Grade Carbon Fiber Tape and Bamboo Fiber Polypropylene Composites. SAMPE JOURNAL. 2023;59(2):22-9.
[5] Yao S-S, Jin F-L, Rhee KY, Hui D, Park S-J. Recent advances in carbon-fiber-reinforced thermoplastic composites: A review. Composites Part B: Engineering. 2018;142:241-50.
[6] Yuan X, Jayaraman K, Bhattacharyya D. Effects of plasma treatment in enhancing the performance of woodfibre-polypropylene composites. Composites Part A: Applied Science and Manufacturing. 2004;35(12):1363-74.
[7] Zhang J, Lin G, Vaidya U, Wang H. Past, present and future prospective of global carbon fibre composite developments and applications. Composites Part B: Engineering. 2022:110463.
[8] Bonhomme J, Argüelles A, Viña J, Viña I. Fractography and failure mechanisms in static mode I and mode II delamination testing of unidirectional carbon reinforced composites. Polymer Testing. 2009;28(6):612-7.
[9] Fu S, Sun Z, Huang P, Li Y, Hu N. Some basic aspects of polymer nanocomposites: A critical review. Nano Materials Science. 2019;1(1):2-30.
[10] Lew C, Chowdhury F, Hosur MV, Netravali AN. The effect of silica (SiO2) nanoparticles and ammonia/ethylene plasma treatment on the interfacial and mechanical properties of carbon-fiber-reinforced epoxy composites. Journal of adhesion science and technology. 2007;21(14):1407-24.
[11] Ma K, Wang B, Chen P, Zhou X. Plasma treatment of carbon fibers: Non-equilibrium dynamic adsorption and its effect on the mechanical properties of RTM fabricated composites. Applied Surface Science. 2011;257(9):3824-30.
[12] Pukanszky B, VÖRÖS G. Mechanism of interfacial interactions in particulate filled composites. Composite Interfaces. 1993;1(5):411-27.
[13] Tiwari S, Sharma M, Panier S, Mutel B, Mitschang P, Bijwe J. Influence of cold remote nitrogen oxygen plasma treatment on carbon fabric and its composites with specialty polymers. Journal of Materials Science. 2011;46:964-74.
[14] Vinodhini J, Sudheendra K, Balachandran M, Bhowmik S. Influence of argon plasma treatment on carbon fibre reinforced high performance thermoplastic composite. High Performance Polymers. 2021;33(3):285-94.
[15] Sharma M, Gao S, Mäder E, Sharma H, Wei LY, Bijwe J. Carbon fiber surfaces and composite interphases. Composites Science and Technology. 2014;102:35-50.
[16] Hull KL, Sayed M, Al-Muntasheri GA. Recent advances in viscoelastic surfactants for improved production from hydrocarbon reservoirs. SPE Journal. 2016;21(04):1340-57.
[17] Mengjin W, Lixia J, Suling L, Zhigang Q, Sainan W, Ruosi Y. Interfacial performance of high-performance fiber-reinforced composites improved by cold plasma treatment: A review. Surfaces and Interfaces. 2021;24:101077.

[18] Sethi S, Ray BC. Environmental effects on fibre reinforced polymeric composites: Evolving reasons and remarks on interfacial strength and stability. Advances in colloid and interface science. 2015;217:43-67.
[19] Brasington A, Sacco C, Halbritter J, Wehbe R, Harik R. Automated fiber placement: A review of history, current technologies, and future paths forward. Composites Part C: Open Access. 2021;6.
[20] Croft K, Lessard L, Pasini D, Hojjati M, Chen J, Yousefpour A. Experimental study of the effect of automated fiber placement induced defects on performance of composite laminates. Composites Part A: Applied Science and Manufacturing. 2011;42(5):484-91.
[21] Heathman N, Koirala P, Yap T, Emami A, Tehrani M. In situ consolidation of carbon fiber PAEK via laser-assisted automated fiber placement. Composites Part B: Engineering. 2023;249:110405.
[22] Rousseau G, Wehbe R, Halbritter J, Harik R. Automated Fiber Placement Path Planning: A state-of-the-art review. Computer-Aided Design and Applications. 2018;16(2):172-203.
[23] Tafreshi OA, Hoa SV, Shadmehri F, Hoang DM, Rosca D. Heat transfer analysis of automated fiber placement of thermoplastic composites using a hot gas torch. Advanced Manufacturing: Polymer & Composites Science. 2019;5(4):206-23.
[24] Li W, Sang L, Jian X, Wang J. Influence of sanding and plasma treatment on shear bond strength of 3D-printed PEI, PEEK and PEEK/CF. International Journal of Adhesion and Adhesives. 2020;100:102614.
[25] Yildirim C, Ulus H, Beylergil B, Al-Nadhari A, Topal S, Yildiz M. Effect of atmospheric plasma treatment on Mode-I and Mode-II fracture toughness properties of adhesively bonded carbon fiber/PEKK composite joints. Engineering Fracture Mechanics. 2023;289:109463.
[26] Jang J, Kim H. Improvement of carbon fiber/PEEK hybrid fabric composites using plasma treatment. Polymer composites. 1997;18(1):125-32.
[27] Zhang Z, Wilson JL, Kitt BR, Flaherty DW. Effects of Oxygen Plasma Treatments on Surface Functional Groups and Shear Strength of Carbon Fiber Composites. ACS Applied Polymer Materials. 2021;3(2):986-95.
[28] Lu C, Qiu S, Lu X, Wang J, Xiao L, Zheng T, et al. Enhancing the interfacial strength of carbon fiber/poly (ether ether ketone) hybrid composites by plasma treatments. Polymers. 2019;11(5):753.
[29] Fitzgibbon A, Pilu M, Fisher RB. Direct least square fitting of ellipses. IEEE Transactions on pattern analysis and machine intelligence. 1999;21(5):476-80.
[30] Song W, Gu A, Liang G, Yuan L. Effect of the surface roughness on interfacial properties of carbon fibers reinforced epoxy resin composites. Applied surface science. 2011;257(9):4069-74.
[31] Park S, Kim J, Park CH. Influence of micro and nano-scale roughness on hydrophobicity of a plasma-treated woven fabric. Textile Research Journal. 2017;87(2):193-207.
[32] Mittal KL. Contact Angle, Wettability and Adhesion, Volume 3: CRC Press; 2003.
[33] Cassie A, Baxter S. Wettability of porous surfaces. Transactions of the Faraday society. 1944;40:546-51.
[34] Machala Z, Tarabová B, Sersenová D, Janda M, Hensel K. Chemical and antibacterial effects of plasma activated water: Correlation with gaseous and aqueous reactive oxygen and nitrogen species, plasma sources and air flow conditions. Journal of Physics D: Applied Physics. 2018;52(3):034002.
[35] Fu Q, Gabriel M, Schmidt F, Müller W-D, Schwitalla AD. The impact of different low-pressure plasma types on the physical, chemical and biological surface properties of PEEK. Dental Materials. 2021;37(1):e15-e22.
[36] Zhang S, Awaja F, James N, McKenzie DR, Ruys AJ. Autohesion of plasma treated semi-crystalline PEEK: Comparative study of argon, nitrogen and oxygen treatments. Colloids and Surfaces A: Physicochemical and Engineering Aspects. 2011;374(1-3):88-95.
[37] Goddard JM, Hotchkiss J. Polymer surface modification for the attachment of bioactive compounds. Progress in polymer science. 2007;32(7):698-725.
[38] Oehr C. Plasma surface modification of polymers for biomedical use. Nuclear Instruments and Methods in Physics Research Section B: Beam Interactions with Materials and Atoms. 2003;208:40-7.

643 [39] Švorčík V, Kotál V, Slepička P, Bláhová O, Špírková M, Sajdl P, et al. Modification of surface
644 properties of polyethylene by Ar plasma discharge. Nuclear Instruments and Methods in Physics
645 Research Section B: Beam Interactions with Materials and Atoms. 2006;244(2):365-72.
646 [40] Chan C-M, Ko T-M, Hiraoka H. Polymer surface modification by plasmas and photons. Surface
647 science reports. 1996;24(1-2):1-54.
648 [41] Yasuda H, Hirotsu T. Critical evaluation of conditions of plasma polymerization. Journal of
649 Polymer Science: Polymer Chemistry Edition. 1978;16(4):743-59.
650 [42] Desmet T, Morent R, De Geyter N, Leys C, Schacht E, Dubruel P. Nonthermal plasma technology
651 as a versatile strategy for polymeric biomaterials surface modification: a review. Biomacromolecules.
652 2009;10(9):2351-78.
653 [43] Korycki A, Carassus F, Tramis O, Garnier C, Djilali T, Chabert F. Polyaryletherketone Based Blends:
654 A Review. Polymers. 2023;15(19):3943.
655 [44] Vieille B, Albouy W, Chevalier L, Taleb L. About the influence of stamping on thermoplastic-based
656 composites for aeronautical applications. Composites Part B: Engineering. 2013;45(1):821-34.
657 [45] Cheng J, Li H-j, Zhang S-y, Xue L-z, Luo W-f, Li W. Failure behavior investigation of a unidirectional
658 carbon–carbon composite. Materials & Design. 2014;55:846-50.
659 [46] Danzi F, Campos PJS, Arteiro A, Dalli D, Furtado C, Chevalier J, et al. Longitudinal failure
660 mechanisms and crack resistance curves of unidirectional thermoplastic composites. Engineering
661 Fracture Mechanics. 2023;282:109147.
662 [47] Morent R, De Geyter N, Desmet T, Dubruel P, Leys C. Plasma surface modification of
663 biodegradable polymers: a review. Plasma processes and polymers. 2011;8(3):171-90.

664